A New Approach to Direct Torque Control of Induction Motor Drives for Constant Inverter Switching Frequency and Torque Ripple Reduction

Yen-Shin Lai, *Member, IEEE* and Jian-Ho Chen

***Abstract*—In this paper a new approach to direct torque control (DTC) of induction motor drive is presented. In comparison with the conventional DTC methods [1], [22] the inverter switching frequency is constant and is dramatically increased, requiring neither any increase of the sampling frequency, nor any high frequency dither signal. The well-developed space vector modulation technique is applied to inverter control in the proposed DTC-based induction motor drive system, thereby dramatically reducing the torque ripple and speed ripple. As compared to the existing DTC approach [2], [23] with constant inverter switching frequency, the presented new approach does not invoke any concept of deadbeat control, thereby dramatically reducing the computations. Experimental results are illustrated in this paper confirming that the proposed DTC method has the above-mentioned features even at the low speed range down to ± 1 r/min.**

***Index Terms*—Direct torque control, induction motor drives, inverter.**

I. Introduction

IT IS well known that the basic concept of direct torque control of induction motor drives is to control both stator flux and electromagnetic torque of machine simultaneously. As demonstrated in [1], [22], [3]–[6], both torque and flux of a DTC-based drive are controlled in the manner of closed-loop system without using current loops in comparison with the conventional vector-controlled drives. In principle, the DTC-based drives require the knowledge of stator resistance only, and thereby decreasing the associated sensitivity to parameter variations. Moreover, the DTC-based drives do not require fulfilling the coordinate transformation between stationary frame and synchronous frame, in comparison with the conventional vector-controlled drives.

Since a DTC-based drive [1], [22] selects the inverter switching states using switching table, neither current controllers nor pulse-width modulation (PWM) modulator is required, thereby providing fast torque response. However, this switching-table-based DTC approach is accompanied by some disadvantages; more details are described as follows.

Manuscript received June 21, 1999. This work was supported by the National Science Council under Grants NSC 88-2213-E-027-014.

Y.-S. Lai is with the Department of Electrical Engineering, National Taipei University of Technology, 1, Sec. 3, Chung-Hsiao E. Rd., Taipei, Taiwan.

J.-H. Chen is with the Institute of Mechatronic Engineering, National Taipei University of Technology, 1, Sec. 3, Chung-Hsiao E. Rd., Taipei, Taiwan.

Publisher Item Identifier S 0885-8969(01)07334-X.

For digital implementation, the system sampling frequency for the calculations of torque and flux should be very fast in order to provide good tracking performance and limit the errors of torque and flux within the specified bands, respectively. The inverter switching frequency, which varies with speed of drives and the associated error bands, is very low in comparison with the system sampling frequency; a sampling frequency of 40 kHz gives the inverter switching frequency about 3 kHz as shown in [7]. Although the inverter switching frequency can be increased by mixing high frequency dither signals with the error signals of torque and flux, respectively, the inverter switching frequency is not constant for small error bands [8] and the difficulty of designing inverter output filter becomes difficult. For the DTC-based drives, the torque ripple is significantly for not invoking the zero inverter switching states; especially at motor start-up [9] or under transient state [10].

Alternatively, space vector modulation (SVM) modulator is incorporated with direct torque control for induction motor drives as shown in [2], [23], [11] to provide a constant inverter switching frequency. Noting that the torque ripple and noise issue for this SVM-based DTC approach are significantly improved for invoking zero inverter switching state within every switching period of inverter control. In [2], [23] a deadbeat controller is used to generate the voltage command of SVM modulator, which requires calculating several complicate equations on-line. In [11], a predictive controller is used to generate the voltage command for inverter control using space vector modulation technique. However, the predictive controller consists of a deadbeat controller, a feed forward controller and two integrators, and no experimental results are presented in the paper.

In this paper, it is intended to solve the issues associated with the conventional switching-table-based DTC drives as mentioned previously in this section. It will be demonstrated in this paper that the inverter switching frequency is increased requiring neither the increase of sampling frequency, nor any dither high frequency dither signal. And, the inverter switching frequency is kept constant without invoking any complicate deadbeat controller. Furthermore, the well-developed space vector modulation technique is applied to inverter control in the proposed DTC-based induction motor drive system, thereby dramatically reducing the torque ripple and speed ripple. Experimental results derived from a test drive system are presented to firmly support the claims of this paper.

0885–8969/01$10.00 © 2001 IEEE

II. Theory

A. Machine Modeling

An induction motor is modeled using voltage and flux equations which are referred to a general reference frame, denoted by the superscript "g" and are shown as follows [12], [13].

Stator Voltage Equation:

$$v_s^g = i_s^g R_s + j\omega_g \lambda_s^g + p\lambda_s^g. \tag{1}$$

Rotor Voltage Equations:

$$0 = i_r^g R_r + j(\omega_g - \omega_r)\lambda_r^g + p\lambda_r^g. \tag{2}$$

Stator Flux Equation:

$$\lambda_s^g = L_s i_s^g + L_m i_r^g. \tag{3}$$

Rotor Flux Equation:

$$\lambda_r^g = L_r i_r^g + L_m i_s^g. \tag{4}$$

Mechanical Equation:

$$T_e - T_L = J_m p\omega_r + B_m \omega_r \tag{5}$$

$$T_e = \frac{3P}{4}(\lambda_{ds}^g i_{qs}^g - \lambda_{qs}^g i_{ds}^g). \tag{6}$$

By referring to a stationary frame, denoted by the superscript "α," which is with d-axis attached on the stator winding of phase "A," the mathematical equations of induction motor can be rewritten as follows.

Stator Voltage Equation:

$$v_s^\alpha = i_s^\alpha R_s + p\lambda_s^\alpha. \tag{7}$$

Rotor Voltage Equations:

$$0 = i_r^\alpha R_r - j\omega_r \lambda_r^\alpha + p\lambda_r^\alpha. \tag{8}$$

Stator Flux Equation:

$$\lambda_s^\alpha = L_s i_s^\alpha + L_m i_r^\alpha. \tag{9}$$

Rotor Flux Equation:

$$\lambda_r^\alpha = L_r i_r^\alpha + L_m i_s^\alpha. \tag{10}$$

Mechanical Equation:

$$T_e - T_L = J_m p\omega_r + B_m \omega_r \tag{11}$$

$$T_e = \frac{3P}{4}(\lambda_{ds}^\alpha i_{qs}^\alpha - \lambda_{qs}^\alpha i_{ds}^\alpha). \tag{12}$$

Substituting (9) and (10) into (12), yields

$$T_e = \frac{3P}{4}\frac{L_m}{\sigma L_s L_r}(\lambda_{ds}^\alpha \lambda_{qr}^\alpha - \lambda_{qs}^\alpha \lambda_{dr}^\alpha) \tag{13}$$

where $\sigma =$ total leakage factor, $\sigma \equiv 1 - (L_m^2/L_s L_r)$.

B. The Conventional Direct Torque Control Approach

The stator flux is by (14), which is derived from (7).

$$\hat{\lambda}_s^\alpha = \int (\hat{v}_s^\alpha - \hat{i}_s^\alpha R_s)\, dt \tag{14}$$

where $\hat{v}_s^\alpha$ and $\hat{i}_s^\alpha$ indicate the measured stator voltage and current, respectively.

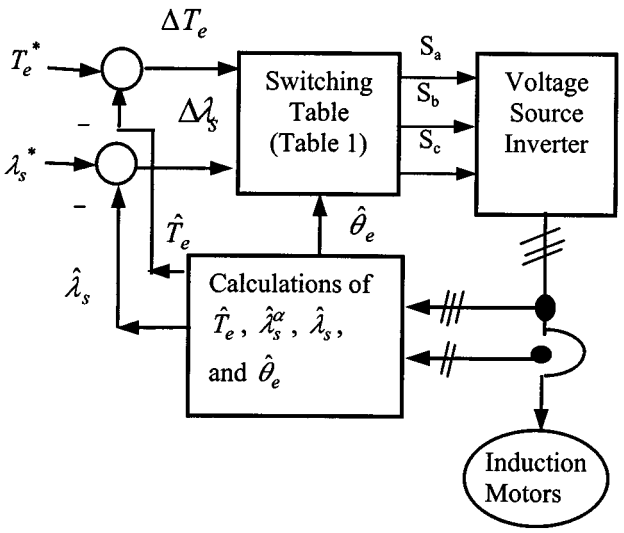

Fig. 1. Block diagram of the conventional direct torque control of induction motor drives.

The electromagnetic torque is calculated by (15), which is derived by (12).

$$\hat{T}_e = \frac{3P}{4}\left(\hat{\lambda}_{ds}^\alpha \hat{i}_{qs}^\alpha - \hat{\lambda}_{qs}^\alpha \hat{i}_{ds}^\alpha\right). \tag{15}$$

Fig. 1 shows the direct block diagram of the conventional direct torque control for induction motor drive. As shown in Fig. 1, the inverter switching states are selected according to the errors of the torque and flux, which are indicated by, ΔT_e and $\Delta\lambda_s$, respectively. Noting that

$$\Delta T_e \equiv T_e^* - \hat{T}_e \tag{16}$$

$$\Delta\lambda_s \equiv \lambda_s^* - \hat{\lambda}_s \tag{17}$$

where

$$\hat{\lambda}_s \equiv \sqrt{\left(\hat{\lambda}_{ds}^\alpha\right)^2 + \left(\hat{\lambda}_{qs}^\alpha\right)^2}. \tag{18}$$

Table I shows the associated inverter switching states for two-level inverter control of the conventional direct torque control approach. As shown in Table I, the inverter switching states are determined by the errors of torque and flux, and the position of stator flux, which is denoted by $\hat{\theta}_e$ and given by

$$\hat{\theta}_e \equiv \tan^{-1}\left[\frac{\hat{\lambda}_{qs}^\alpha}{\hat{\lambda}_{ds}^\alpha}\right]. \tag{19}$$

The definition of sectors is shown in Fig. 2, in which the position relationship between stator voltage vector and stator flux vector is clearly identified. As shown in Fig. 2, the stator flux vector, λ_s^α, lags the associated stator voltage vector, v_s^α, by 90 degrees if the voltage drop across the stator resistance shown in (14) is negligible.

Noting that a speed controller can be added to Fig. 1 to generate the torque command, and therefore fulfill a DTC-based adjustable speed drive as illustrated in Fig. 3. As shown in Fig. 3, the shaft speed of induction motor drive can be derived using

TABLE I
SWITCHING TABLE FOR THE CONVENTIONAL DIRECT TORQUE CONTROL OF INDUCTION MOTOR DRIVES

	$\hat{v}_s^\alpha$	Sector 1	Sector 2	Sector 3	Sector 4	Sector 5	Sector 6
	$\hat{\theta}_e$	$[\frac{-\pi}{2}, \frac{-\pi}{6}]$	$[\frac{-\pi}{6}, \frac{\pi}{6}]$	$[\frac{\pi}{6}, \frac{\pi}{2}]$	$[\frac{\pi}{2}, \frac{5\pi}{6}]$	$[\frac{5\pi}{6}, \frac{7\pi}{6}]$	$[\frac{7\pi}{6}, \frac{3\pi}{2}]$
Decrease	Increase Torque	100	110	010	011	001	101
Flux	Decrease Torque	011	001	101	100	110	010
Increase	Increase Torque	110	010	011	001	101	100
Flux	Decrease Torque	001	101	100	110	010	011

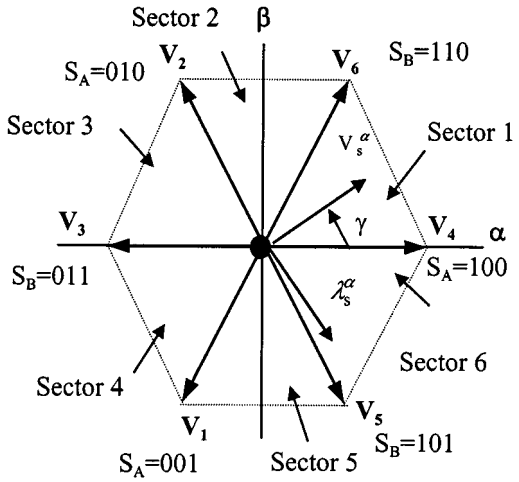

Fig. 2. Relationship between stator voltage vector and flux vector.

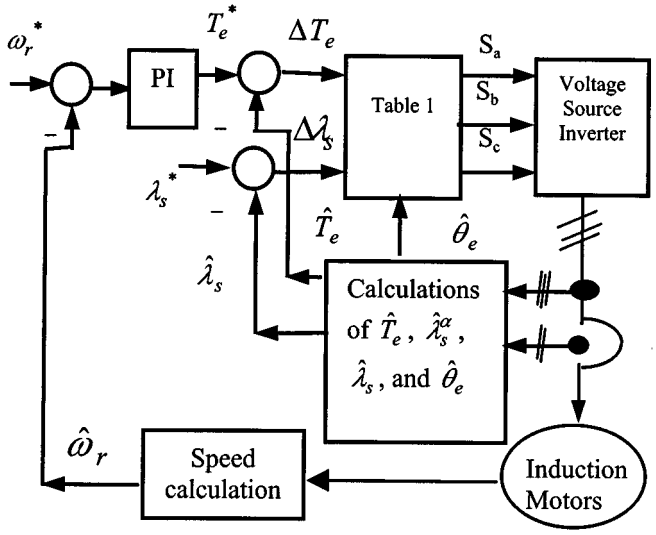

Fig. 3. Block diagram of a DTC-based adjustable speed drive.

an encoder in a closed-loop system or by the speed estimation skills in a sensorless system.

The phase voltages and the associated stator voltage vector shown in (14) are estimated using the scheme shown in [14], [15] and are summarized in (20) and (21).

$$\hat{v}_{an} = \frac{V_{\rm dc}}{3}(2S_a - S_b - S_c)$$
$$\hat{v}_{bn} = \frac{V_{\rm dc}}{3}(-S_a + 2S_b - S_c) \quad (20)$$
$$\hat{v}_{cn} = \frac{V_{\rm dc}}{3}(-S_a - S_b + 2S_c)$$
$$\hat{v}_{ds}^{\alpha} = \frac{V_{\rm dc}}{3}(2S_a - S_b - S_c)$$
$$\hat{v}_{qs}^{\alpha} = \frac{V_{\rm dc}}{\sqrt{3}}(S_b - S_c) \quad (21)$$

where

$\hat{v}_{an}$, $\hat{v}_{bn}$, and $\hat{v}_{cn}$ phase voltages;
S_a, S_b, and S_c denote the inverter switching states, in which $S_i = 1$ $(i = a, b, c)$, if the upper leg switch is on and $S_i = 0$ $(i = a, b, c)$, if the upper leg switch is off;
$V_{\rm dc}$ is the dc link voltage;
$\hat{v}_{ds}^{\alpha}$, $\hat{v}_{qs}^{\alpha}$ two-axis stator voltage in the stationary frame.

Noting that the field oriented control approach invokes the concept of *transforming* the stationary quantities into synchronous ones and *orienting* the referred flux along the d-axis of the *synchronous* frame. More details about the discussion of field oriented control can be found in [12], [13]. In contrast the direct torque control (DTC) shown in Fig. 3 [1], [22], [2], [23], [3]–[11] does *not* invoke any of the above-mentioned works for field oriented control; more details about the DTC can be found in [1], [22], [2], [23], [3]–[11]. As shown in [1], [22], [2], [23], [3]–[11] "θ_e," the position of stator flux, is essential to inverter switching control.

C. Conventional Space Vector Modulation Techniques

As shown in Fig. 2, the switching states of inverter control include eight switching states; six of them, (100), (010), (001), denoted by S_A, and (110), (011) and (101), represented using S_B, are named active switching states, and (000) and (111), denoted

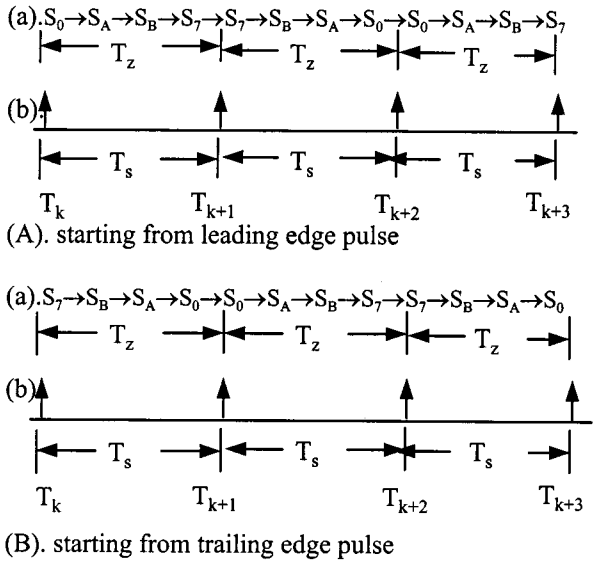

Fig. 4. (a) Switching patterns. (b) Sampling instants for SVM technique.

by S_0 and S_7, respectively. The vector times associated with the switching states are shown in (22) [16], [24] and the switching pattern in one carrier period is shown in Fig. 4.

$$\begin{aligned} T_A &= T_z a \frac{2}{\sqrt{3}} \sin\left(\frac{\pi}{3} - \gamma\right) \\ T_B &= T_z a \frac{2}{\sqrt{3}} \sin(\gamma) \\ T_0 &= T_7 = 0.5(T_z - T_A - T_B) \end{aligned} \tag{22}$$

where $a = V_s^{\alpha *}/(P_k V_{\rm dc})$, $P_k = 2/3$.

Noting that zero switching states, (000) and (111), are included in the switching pattern in a sampling period as shown in Fig. 4. In a sampling period the zero switching states, (000) and (111), with the same vector times, are placed at two edges, respectively. It has been demonstrated [17] that the Total Harmonic Distortion (THD) associated the space vector modulation technique is approximate to that of an optimal PWM technique; and therefore the torque ripple can be reduced in comparison with other three-phase modulation techniques. In the linear modulation range, the inverter switching frequency is constant and is 50% of the sampling frequency. The details about these advantages will be highlighted later in this paper as compared with the switching table technique of the conventional DTC-based system.

D. New DTC-Based Drives

It is well known that the principle of vector control of induction motor drive is to align the flux and torque current along the d-axis and q-axis of the reference fame, respectively. And therefore, the torque can be controlled by the associated current component, once the flux is kept constant. In contrast, as mentioned previously in this paper, the fundamental idea of direct torque control *is to control both the torque and the magnitude of flux within the associated error bands in real time. These control goals can be achieved by selecting the inverter switching states according to the errors of torque and flux.*

Therefore the main theme of direct torque control is to regulate the torque and magnitude of flux directly without invoking any concept of field orientation. Following this essential concept, Fig. 5 shows the block diagram of the new DTC-based induction motor drives. As shown in Fig. 5, two proportional-integral (PI) type controllers regulate the flux amplitude and torque, respectively. Therefore, *both the torque and the magnitude of flux are under control, thereby generating the voltage command for inverter control*. Noting that no decoupling mechanism is required since the flux magnitude and torque can be regulated by the PI controllers. Experimental results derived from a test induction motor drive will be given later in this paper to strongly support this point of view.

As shown in Fig. 5, the inverter is controlled by the SVM technique [16], [24] using Symmetrical Regular-Sampling technique [18]. Therefore, the inverter switching frequency is significantly increased, and the associated torque ripple and current harmonics can be dramatically reduced, in comparison with the conventional switching-table-based DTC drives. More details of these merits of the new DTC drives over the conventional approach are clearly analyzed in next section and will be supported by the experimental results shown later in this paper.

E. Advantages of the New DTC-Based Drives

It is well known that for conventional DTC approach, no inverter leg changes switching state during a sampling period. Due to this fact, *the inverter switching frequency is less than that of sampling frequency* and the associated torque ripple is also significant for low sampling frequency control. As reported in [7], the sampling is increased up to 40 kHz (25 μsec of sampling period) at the cost of using dedicated high performance hardware; however, the inverter switching frequency is about 3 kHz.

Fig. 6 illustrates the PWM pulses for the SVM technique [16], [24] using Asymmetrical Regular-Sampling technique. As shown in Fig. 6, the inverter switching frequency is 50% of sampling frequency. For Asymmetrical Regular-Sampled SVM technique, the zero switching states, (000) and (111), are placed in the edges of switching pattern in every sampling period. It has been demonstrated [17] that the Total Harmonic Distortion (THD) of the space vector modulation technique with switching patterns as shown in Fig. 6, is approximate to that of an optimal PWM technique; and therefore the torque ripple can be reduced.

To increase the inverter switching frequency for the same sampling frequency, the Symmetrical Regular-Sampled SVM technique with switching patterns as shown in Fig. 7 is used for inverter control of the new DTC-based drive. The inverter switching frequency is constant and is equal to sampling frequency.

Therefore, for the same sampling frequency, in comparison with the conventional switching-table-based DTC drive, the new DTC-based drive dramatically increases the inverter switching frequency; and thereby significantly reducing the torque ripple. Experimental results will be shown later in this paper to confirm this analysis.

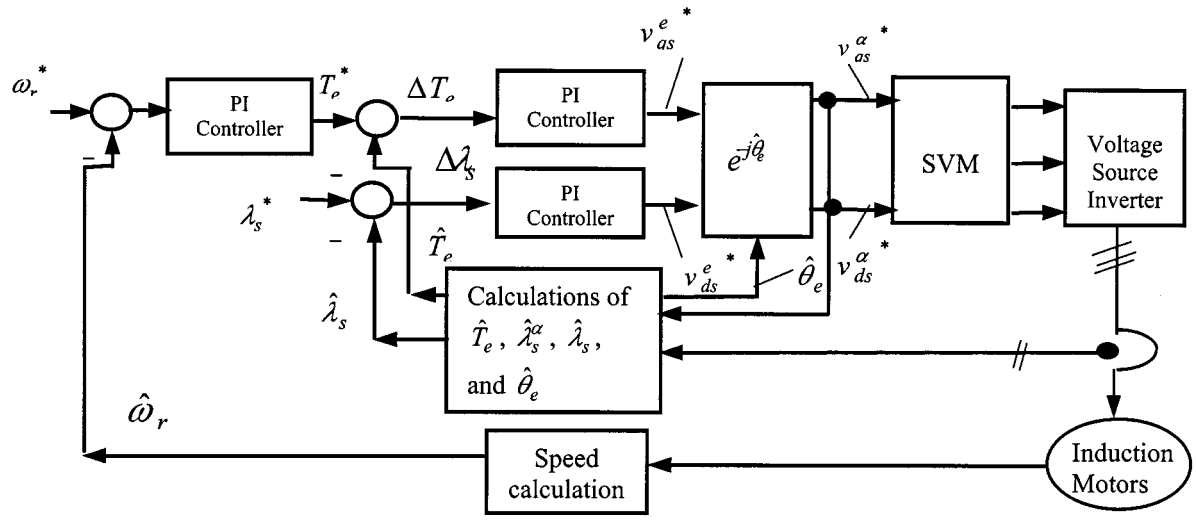

Fig. 5. Block diagram of the proposed DTC-based induction motor drives.

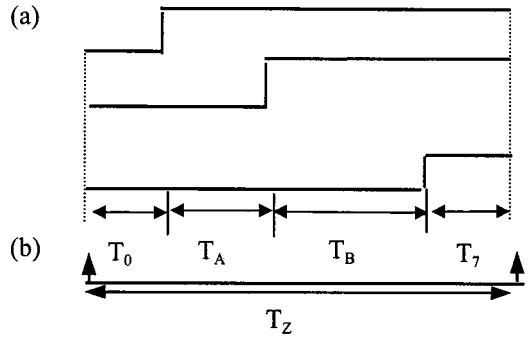

Fig. 6. Illustration of PWM pulses of inverter control, asymmetrical regular-sampled SVM technique. (a) Switching patterns. (b) Sampling instant.

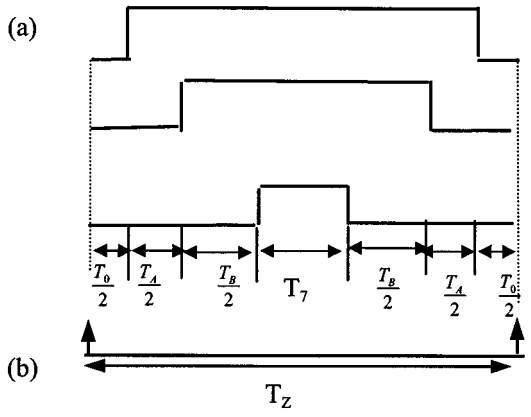

Fig. 7. Illustration of PWM pulses of inverter control for the new DTC-based drive system; asymmetrical regular-sampled SVM technique. (a) Switching patterns. (b) Sampling instant.

III. Implementation and Experimental Results

A PC-based induction motor drive is used as the test system. The system consists of a 586 PC, an IGBT inverter, and an induction motor with a 1000 pulses/rev encoder. More details about the specification and parameters of the induction motor are listed in the Appendix.

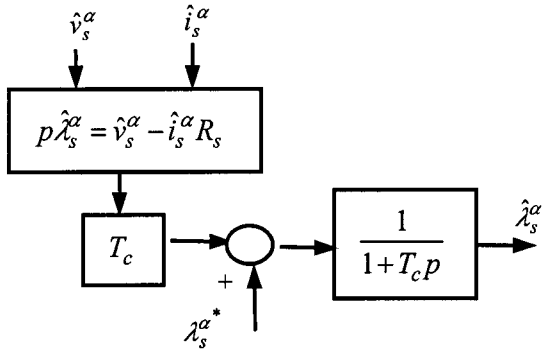

Fig. 8. Stator flux estimation for implementation.

It is well known that both switching losses and sampling frequency of controller of drives limit the inverter switching frequency. The discussion about these two topics and the related solutions can be found in [20]–[22]. Since the inverter switching frequency for conventional DTC schemes depends upon the hysteresis band and is not constant, the experimental results for comparisons are conducted based upon the same sampling frequency of controller of drives.

Noting that the accuracy of the estimated stator flux using (14) will be affected by the initial conditions caused by the pure integral operation. The signals of voltage and current are dominated by the harmonics at low speed range, thereby significantly affecting the accuracy of estimation. A stator flux estimation scheme as shown in Fig. 8 and (23), which is similar to that proposed in [19] for rotor flux estimation, is used to overcome the above-mentioned issue for stator flux estimation.

As shown in Fig. 8 at high speed range, the estimated stator flux is approximate to the value shown in (14) while without invoking any integral operation. At low speed range, in which the current and voltage signals are dominated by the harmonics, the

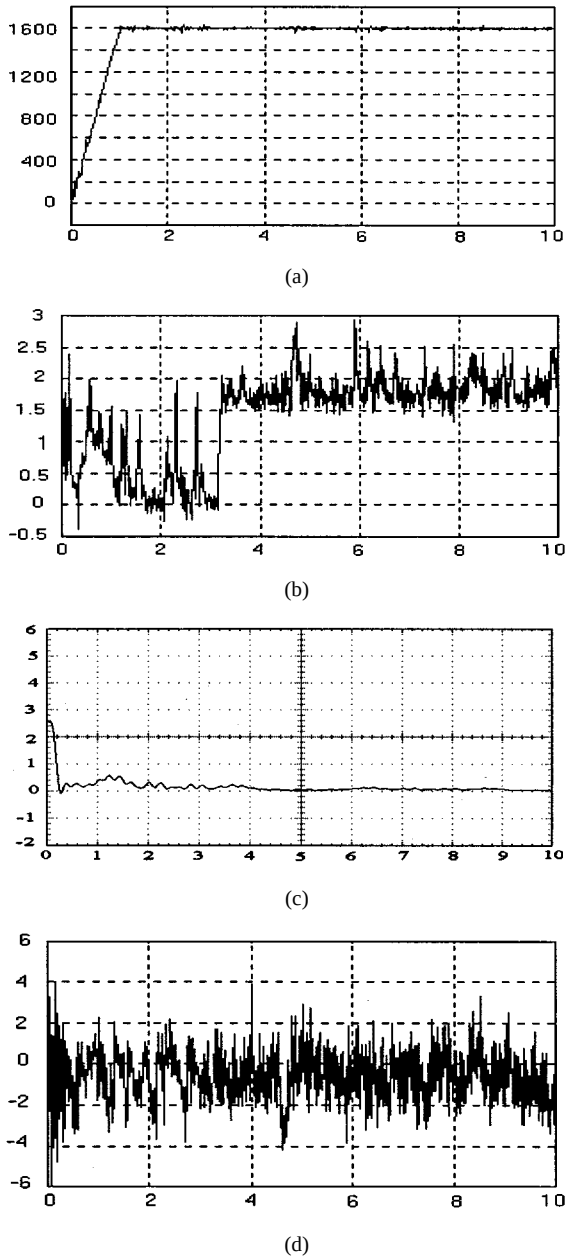

Fig. 9. Experimental results of the conventional DTC system. (a) Speed response; x-axis in sec, y-axis in rpm. (b) Estimated torque; x-axis in sec, y-axis in Nt-m. (c) Spectrum of inverter switching pulses; x-axis in kHz, y-axis in volt. (d) Phase current; x-axis in sec, y-axis in amp.

command value of stator flux is used instead, thereby providing satisfied accuracy even at low speed range.

$$\begin{aligned}\hat{\lambda}_s^{\alpha} &= \int \left(\hat{v}_s^{\alpha} - \hat{i}_s^{\alpha} R_s\right) dt \\ &= \frac{1}{p}\left(\hat{v}_s^{\alpha} - \hat{i}_s^{\alpha} R_s\right) \\ &\approx \frac{1}{1+T_c p}\left[T_c\left(\hat{v}_s^{\alpha} - \hat{i}_s^{\alpha} R_s\right)\right] + \frac{1}{1+T_c p}\lambda_s^{*} \end{aligned} \quad (23)$$

where $T_c = (1/2\pi f_c)$ and $f_c =$ cut-off frequency of filter.

The experimental results are measured using the following equipment.

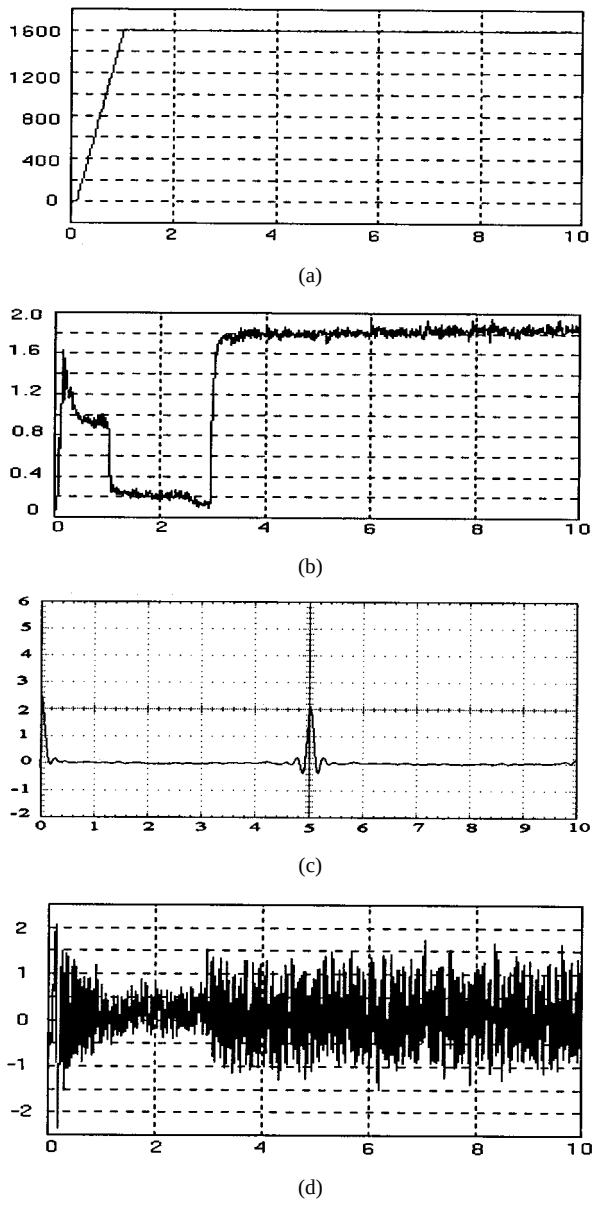

Fig. 10. Experimental results of the proposed DTC system. (a) Speed response; x-axis in sec, y-axis in rpm. (b) Estimated torque; x-axis in sec, y-axis in Nt-m. (c) Spectrum of inverter switching pulses; x-axis in kHz, y-axis in volt. (d) Phase current; x-axis in sec, y-axis in amp.

oscilloscope: Tektronix TDS 460 A
voltage differential probe: SI-900

Fig. 9 shows the experimental results for the conventional DTC system as shown in Fig. 3; the error bands of torque and flux are 2% of rated torque and nominal flux value, respectively. The experiment is conducted at a profile of 1600 r/min and a step load, 1.8 N-m which is 45% of rated torque, is applied at $t = 3$ sec. The sampling frequency is 5 kHz and the inverter switching frequency is less than 5 kHz as shown in Fig. 9(c). As shown in Fig. 9(a) and (b), the speed and torque ripple is significant.

Fig. 10 shows the experimental results for the proposed DTC system as shown in Fig. 5. The experimental is conducted using the same profile as that for the experimental results shown in Fig. 10. Noting that the SVM technique is Symmetrical SVM technique, which gives the inverter switching frequency equal

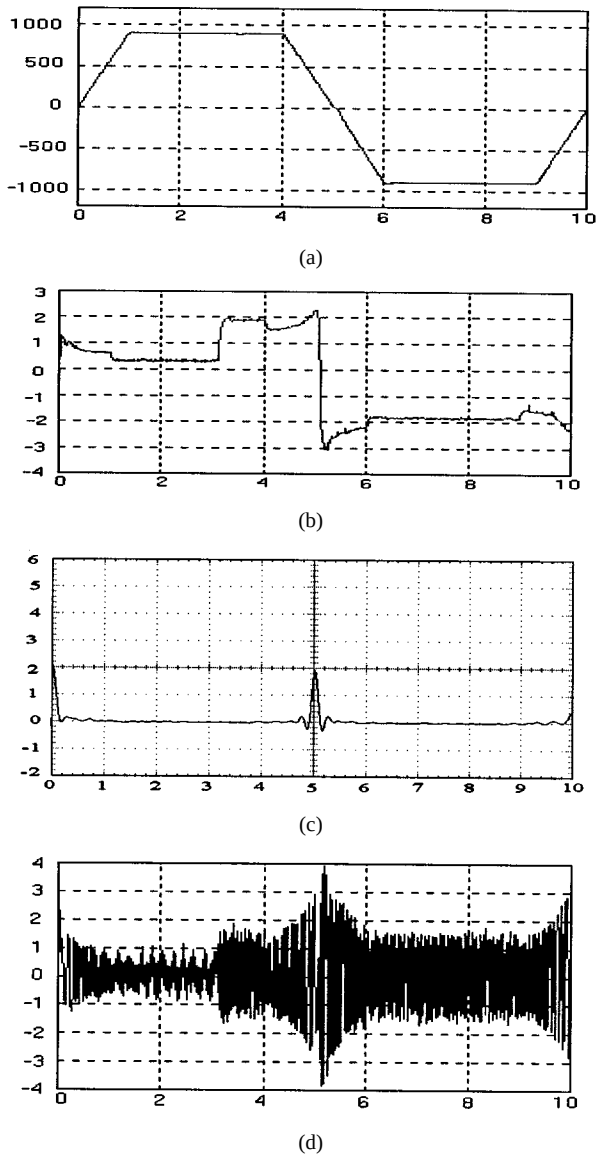

Fig. 11. Experimental results of the proposed DTC system; ± 900 r/min. (a) Speed response; x-axis in sec, y-axis in rpm. (b) Estimated torque; x-axis in sec, y-axis in Nt-m. (c) Spectrum of inverter switching pulses; x-axis in kHz, y-axis in volt. (d) Phase current; x-axis in sec, y-axis in amp.

to that of sampling frequency. As shown in Fig. 10(c), the first dominant harmonic cluster locates at 5 kHz, indicating that the inverter switching frequency is 5 kHz.

In comparison with Fig. 9(c) for the conventional DTC system, the proposed method indeed increases the inverter switching frequency. As shown in Fig. 10(c), the inverter switching frequency is constant and depends on the sampling frequency only. As shown in Fig. 10(a) and (b), the speed and torque ripple is dramatically reduced as compared with those shown in Fig. 9(a) and (b) for the conventional DTC system. Similar remarks can be derived for other speed range and load conditions.

The second experiment is conducted at a speed profile of ± 900 r/min. The profile accelerates from 0 r/min to 900 r/min in 1 s and decelerates from 900 r/min to -900 r/min during 4 s to 6 s. A step load, about 50% of rated torque, is applied at $t = 3$ sec. Fig. 11 shows the associated experimental results.

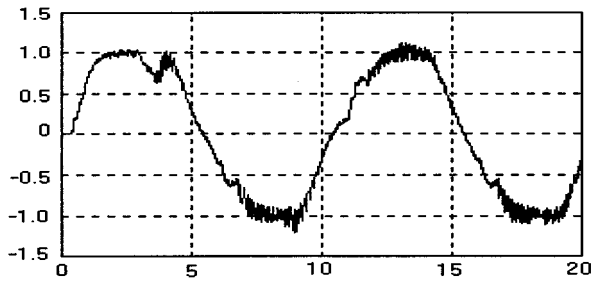

Fig. 12. Experimental results of the proposed DTC system; ± 1 r/min; x-axis in sec, y-axis in rpm.

As shown in Fig. 11(a) and (b), the torque and speed ripples are trivial, and the inverter switching frequency is constant as demonstrated in Fig. 11(c).

The performance of the proposed DTC drive system at low speed region has been further explored by experimental results. The experiment is conducted at a speed profile of ± 1 r/min. A step load, 50% of rated torque, is applied at $t = 3$ sec. Fig. 12 shows the associated experimental results. As shown in Fig. 12, the speed ripples is trivial even at such a low speed range.

IV. Conclusion

In this paper, a new direct torque control method is presented and its merits over the conventional DTC approach are confirmed by the experimental results. The features of the proposed direct torque control method include 1) providing constant inverter switching frequency, 2) dramatically increasing the inverter switching frequency without requiring any high frequency dither signal, 3) significantly reducing the torque and speed ripple. Experimental results are illustrated in this paper confirming that the proposed DTC method has the above-mentioned features even at the low speed range down to ± 1 r/min.

The proposed DTC approach is verified using a two-level inverter system, it can also be applied to a three-level inverter system and multi-level inverter system. The authors wish to report more details of the experimental results in these aspects in the near future.

Appendix

List of motor specification and parameters

220 V, 3ϕ, 1 HP 0.75 KW, 4 poles, 1680 rpm.

Motor Parameters

$R_s = 9.6\ \Omega$
$R_r = 7.008\ \Omega$
$L_r = L_s = 0.8896$ H
$L_m = 0.8794$ H
$J = 0.009$ kg-m^2
$B = 0.008\,25$ Nt-m/rad/s

References

[1] I. Takahashi and Y. Ohmori, "High-performance direct torque control of induction motor," *IEEE Trans. Ind. Appl.*, vol. 25, no. 2, pp. 257–264, 1989.

[2] T. G. Habetler, F. Profumo, M. Pastorelli, and L. M. Tolbert, "Direct torque control of induction machines using space vector modulation," *IEEE Trans. Ind. Appl.*, vol. 28, no. 5, pp. 1045–1053, 1992.

[3] M. Depenbrock, "Direct-self control of inverter-fed induction machine," *IEEE Trans. Power Electrons*, vol. 3, no. 4, pp. 420–429, 1988.
[4] ——, "Direct self control for high dynamics performance of inverter feed a.c. machines," *ETZ Archiv.*, vol. 7, no. 7, pp. 211–218, 1985.
[5] ——, "Direct-self control of the flux and rotary moment of a rotary-field machine," US Patent 4 678 248, 1987.
[6] P. Tiitinen, "The next generation motor control method, DTC direct torque control," in *Proceedingss of the IEEE Intl. Conf. on Power Electronics, Drives, and Energy Systems for Industrial Growth*, 1996, pp. 37–43.
[7] J. N. Nash, "Direct torque control, induction motor vector control without an encoder," *IEEE Trans. Ind. Appl.*, vol. 33, no. 2, pp. 333–341, 1997.
[8] T. Noguchi, M. Yamamoto, S. Kondo, and I. Takashi, "High frequency switching operation of PWM inverter for direct torque control of induction motor," in *Conference Record IEEE IAS Annual Meeting*, 1997, pp. 775–780.
[9] M. P. Kazmierkowski and A. B. Kasprowicz, "Improved direct torque and flux vector control of PWM inverter-fed induction motor drives," *IEEE Trans. Ind. Electron.*, vol. 42, no. 4, pp. 344–349, 1995.
[10] D. Casadei, G. Grandi, G. Serra, and A. Tani, "Switching strategies in direct torque control of induction machines," in *Proc. of the Internal Conference on Electrical Machines (ICEM)*, 1994, pp. 204–209.
[11] G. Buja, D. Casadei, and G. Serra, "Direct stator flux and torque control of an induction motor: Theoretical analysis and experimental results," in *Proceedings of the IECON '98*, vol. 1, 1998, pp. T50–T64.
[12] G. R. Slemon, "Modeling of induction machines for electric drives," *IEEE Trans. Ind. App.*, vol. 25, no. 6, pp. 1126–1131, 1989.
[13] Y. S. Lai, "Modeling and vector control of induction machines—A new unified approach," in *Proc. of the IEEE Power Engineering Society Winter Meeting*, 1999, pp. 47–52.
[14] T. C. Green and B. W. Williams, "Derivation of motor line-current waveforms from the dc link current of an inverter," *Proc. Inst. Elect. Eng.*, pt. B, vol. 136, no. 4, pp. 196–204, 1989.
[15] Y. Xue, X. Xu, T. G. Habetler, and D. M. Divan, "A stator flux-oriented voltage source variable-speed drive based on dc link measurement," *IEEE Trans. Ind. Appl.*, vol. 27, no. 5, pp. 962–969, 1991.
[16] H. W. van der Broeck, H. C. Skudelny, and G. V. Stanke, "Analysis and realization of a pulsewidth based on voltage space vectors," in *IEEE IAS Ann. Meet.*, 1986, pp. 244–251.
[17] S. R. Bowes and Y. S. Lai, "The relationship between space vector modulation and regular-sampled pulse-width modulation," *IEEE Trans. Industrial Electronics*, vol. 44, no. 5, pp. 670–679, 1997.
[18] S. R. Bowes, "New sinusoidal pulsewidth-modulated inverter," *Proc. IEE*, vol. 122, no. 11, pp. 1279–1285, 1975.
[19] T. Ohtani and H. Takasaki, "High performance vector control of induction motor using torque-producing current," in *IPEC Conference Record*, 1990, pp. 61 and 84–90.
[20] Y. S. Lai and S. R. Bowes, "A universal space vector modulation based on regular-sampled pulse-width modulation," in *Proc. of the IEEE IECON*, 1996, pp. 120–126.
[21] ——, "Investigations into optimising high switching frequency regular-sampled PWM for drives and static power converter," in *IEE Proc. Electr. Power Appl.*, vol. 143, 1996, pp. 281–292.
[22] I. Takahashi and Y. Ohmori, "High-performance direct torque control of induction motor," in *Conference Record IEEE IAS Annual Meeting*, 1985, pp. 495–502.
[23] T. G. Habetler, F. Profumo, M. Pastorelli, and L. M. Tolbert, "Direct torque control of induction machines using space vector modulation," in *Conference Record IEEE IAS Annual Meeting*, vol. 1, 1991, pp. 428–435.
[24] H. W. van der Broeck, H. C. Skudelny, and G. V. Stanke, "Analysis and realization of a pulsewidth based on voltage space vectors," *IEEE Trans. Ind. Appl.*, vol. 24, no. 1, pp. 142–150, 1988.

Yen-Shin Lai (M'96) received the M.S. degree from the National Taiwan University of Science and Technology, Taipei, Taiwan, and the Ph.D. degree from the University of Bristol, Bristol, England, U.K., both in electronic engineering. In 1987, he joined the National Taipei University of Technology, Taipei, Taiwan, as a Lecturer and is currently a Professor.

He received the *John Hopkinson Premium* for the session 1995/1996 from the *Institute of Electrical Engineers (IEE)*.

His research interests include design of microprocessor-based systems, development of PWM techniques, and drives and converter control.

Jian-Ho Chen received the B.S. degree in electrical engineering, from the National Taiwan University of Science and Technology, Taipei, Taiwan, and is currently working for the M.S. degree in the Institute of Mechatronic Engineering, National Taipei University of Technology, Taipei, Taiwan.

His research interests include inverter control and PC-based control.